ACS OMEGA

http://pubs.acs.org/journal/acsodf

Article

Synthesis of Higher Alcohols from Syngas over a K-Modified CoMoS Catalyst Supported on Novel Powder and Fiber Commercial Activated Carbons

Mohamed E. Osman,* Vladimir V. Maximov, Tshepo D. Dipheko, Tatiana F. Sheshko, Alexander G. Cherednichenko, Pavel A. Nikulshin, and Victor M. Kogan

Cite This: *ACS Omega* 2022, 7, 21346−21356

Read Online

ACCESS | Metrics & More | Article Recommendations | Supporting Information

ABSTRACT: In the present study, a series of K-modified CoMoS catalysts with compositions of 10% K, 3.6% Co, and 12 wt % Mo supported over novel commercial activated carbons such as powder materials (DAC and OBC-1) and fiber materials (fabric active sorption (TCA) and nonwoven activated material (AHM)) were prepared and characterized by Brunauer-Emmett-Teller (BET), X-ray fluorescence (XRF), scanning electron microscopy (SEM), SEM−energy dispersive X-ray (EDX), and transmission electron microscopy (TEM). The catalytic activities for higher alcohol synthesis from syngas, conducted at T = 300−360 °C, P = 5 MPa, GHSV = 760 L h^{-1} (kg cat)$^{-1}$, and H_2/CO = 1.0, were investigated. Cat-TCA and Cat-AHM have shown a filamentous morphology with a strip axial arrangement and that a few longitudinal grooves and many irregular particles are distributed on the fiber surfaces. The degree of entanglement of the strip axial arrangement in AHM was found to be more than that in TCA, thus leading to form tangled MoS_2 slabs on AHM and long linear slabs on TCA with long rim sites. The obtained results revealed that the CO conversion increases in the order Cat-TCA < Cat-OBC-1 < Cat-DAC < Cat-AHM. Ethanol, propanol-1, and methanol are the most predominant alcohol products in the collected liquid products, with the byproducts containing mainly butanol-1, isobutanol, amyl alcohol, and isoamyl alcohol. Cat-DAC and Cat-OBC-1 show higher selectivity toward C_{3+}, C_{4+}, propanol-1, butanol-1, isobutanol, and amyl alcohol-1 than Cat-TCA and Cat-AHM. For powdered activated carbons, microporous catalysts inhibited isomerization because the catalyst that contains the highest micropores (Cat-DAC) produced a considerable amount of linear alcohols compared with Cat-OBC-1.

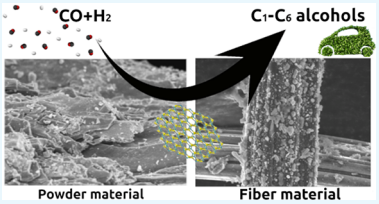

1. INTRODUCTION

Higher alcohol synthesis (HAS) from syngas remains a cost-effectively appealing technique for the production of chemicals and fuels.[1] Several researchers created numerous catalytic techniques for HAS through the hydrogenation of carbon monoxide. From these studies, the catalysts for HAS are classified into two groups:[2−8] (i) modified methanol synthesis catalysts that are used in the production of methanol and branched alcohols and synthesis of straight-chain alcohols, such as transition metal sulfide catalysts (TMSs), which are more attractive due to their good resistance to the poisoning of sulfur,[9,10] and (ii) Co/Cu-based catalysts. Comparatively, molybdenum sulfide based catalysts showed a high proportion of HAS from syngas at lower pressure and high temperature compared with other catalytic systems.[11]

Nonpromoted MoS_2 catalysts exhibit hydrocarbon selectivity in syngas conversion to organic products.[12] However, as Dow Chemical first revealed[13] and Union Carbide showed,[14] high selectivity to HAS can be achieved when MoS_2 is promoted with alkali metal. To synthesize alcohols, MoS_2 must be doped with alkali. With alkali/MoS_2 catalysts, primarily linear primary alcohols are produced, while short hydrocarbons, particularly methane, are the dominant byproducts. Alkali metals impede hydrogenation, promote the active sites responsible for alcohol synthesis,[15−17] as well as increase the length of the MoS_2 slab and the stacking degree.[18,19] To shift the product distribution toward higher alcohols, group VIII promoters such as Co, Ni, Fe, and Rh are frequently added to the catalyst.[20−23] These promoters work as electron density acceptors on the S-edge of the MoS_2-crystallites, which deactivate the sulfur-edge and decrease the adsorption of hydride hydrogen, also leading to increase selectivity toward alcohols at the cost of hydrocarbon selectivity.[15] Previously, the reaction network of alcohol formation on $KCoMoS_2$ catalysts has been investigated.[15]

Catalysts supported on carbon materials have higher activity than those based on metal oxides (Al_2O_3, SiO_2, MgO, ZrO_2), according to several researches.[24−26] The majority of these studies interpret the activity of carbon materials as a result of the weak interaction between the carbon and the KCoMoS

Received: May 17, 2022
Accepted: May 26, 2022
Published: June 6, 2022

active phase, as well as the low acidity compared to metal oxides, which has a positive effect on the selectivity toward alcohols. TMS-based catalysts with high activity and selectivity can be synthesized using a variety of supports that affect the morphology, electron properties, and dispersion of the formed active phase.[27] In the fine chemical industry, activated carbons (ACs) are broadly used as a catalyst support due to their specific properties, such as high stability at high reaction pressures and temperatures,[28−30] larger surface area and porosity, resistance to acidic and basic conditions, and minimal interaction between the support material and active phase.[31,32] In addition, because of the delocalized π electronics, electronic conductivity is an important property of AC.[33] Being microporous (<2 nm), normal activated carbons cause pore plugging due to the formation of coke and deactivation of the sulfided catalyst, which result in transport limitation in the catalytic reaction.[34] Internal diffusion issues can be avoided by using mesoporous supports with pore diameters ranging from 2 to 50 nm. The majority of HAS research has been conducted using microporous AC supported catalysts with significantly smaller surface areas (350−820 m^2/g) than commercially available activated carbons (950 m^2/g and higher), and the long-term activity of these supported catalysts does not meet commercial levels. Depending on the support's textural properties, such as pore volume, surface area, and average pore diameter, the extent of adsorption, morphology, reduction, and selectivity properties of the active phase can be significantly influenced.[35] Surisetty *et al.*[36] investigated the role of microporous and mesoporous activated carbons in the production of alcohols from syngas using trimetallic TMS catalysts and discovered that mesoporous AC has a higher activity than microporous AC. Rather than surface area or pore volume, they believe that CO conversion and alcohol yield are related to the textural properties of the support, such as pore size and microporosity. The researchers found that there is less dispersion on mesoporous MWCNTs than on microporous ACs.

Herein, we studied the effect of two types of novel commercial activated carbons for HAS from synthesis gas over a K-modified $KCoMS_2$ catalyst; besides, the catalytic activity was compared with recent supports that have commercial levels.

2. MATERIALS AND METHODS

2.1. Preparation of Supports and Catalysts. *2.1.1. Preparation of the Commercial Activated Carbons.* Activated carbon DAC (commercial trademark ДАСАС) was obtained from anthracite (hard coal) by the preparation of dough, granulation, carbonization, and gas−vapor activation. Activated carbon OBC-1 (commercial trade mark УУПС-1С-1) was manufactured based on carbonaceous composition prepared from gas−vapor activation at 850−900 °C. Fabric active sorption (TCA) is an elastic sorbent obtained by heat treatment of a technical fabric, which has been previously impregnated with chemical compounds. It was formed as canvases with the following dimensions: length 20 m, width 0.55 m, and thickness 0.6 mm. The nonwoven activated material (AHM) was produced by the heat treatment of a nonwoven needle-punched material based on viscose fibers and Milton fibers. The parameters of the active layer are an aerodynamic resistance of 10 Pa, surface density of 120 g/m^2, and thickness of 1.0−3.5 mm.[37]

2.1.2. Preparation of Supported $KCoMoS_2$ Catalysts. The catalysts were synthesized by the incipient wetness impregnation of the support. Active phase precursors such as cobalt acetate, ammonium heptamolybdate tetrahydrate, and potassium hydroxide were used. The prepared active phase was dried under air condition at 80 °C for 2 h and at 100 °C for 5 h. Finally, prepared samples were sulfidized in an autoclave using crystalized sulfur (1: 4, catalyst/sulfur, respectively) at 370 °C under H_2 at 6.0 MPa for 1 h. The composition of the tested catalysts is presented in Table 1. The wt % of K, Co, Mo, and support was controlled as 10, 3.7, 12, and 74.3%, respectively.

Table 1. Elemental Compositions of Supported Catalysts

	targeted composition (wt %)			measured composition (wt %)		
catalyst	K	Mo	Co	K	Mo	Co
$KCoMoS_2$-DAC	10	12	3.7	8.5	11.9	3.7
$KCoMoS_2$-OBC-1	10	12	3.7	8.4	15.8	3.9
$KCoMoS_2$-TCA	10	12	3.7	11.3	13.9	4.2
$KCoMoS_2$-AHM	10	12	3.7	11.1	15.1	4.6

2.2. Characterization of Carriers and Catalysts. The Quantachrome Nova 1200e at 77 K and N_2 adsorption and desorption isotherms were used to study support and catalyst textural characteristics. The test was performed with 0.1 g of each sample and calibrated sample cells. Before degassing, sulfided samples were kept under hydrogen flow for 3 h. The sulfide samples were degassed at 250 °C for 4 h at 10^{-4} mm Hg. The specific surface area was determined using the BET equation. The total pore volume was investigated at a relative pressure P/P0 = 0.99. The mesopore size distribution was calculated from the desorption branch of the isotherm using the Barrett, Joyner, and Halenda (BJH) method.[38] According to the BJH method, the mesopore volume was calculated as the cumulative pore volume during desorption (considering the adsorption film thickness on the mesopore surface). To determine the micropore volume in the samples, the t-plot method was used[38] and the mesopore volumes and total pore were compared. Volume and pore size values are summarized in Table 1.

The elementary composition of the sulfided catalysts was investigated using a Shimadzu EDX-7000 X-ray fluorescence spectrometer. All samples were crushed before measurements. The conditions of analysis were as follows: voltage: 15−50 kV, tube current: 8−200 mA, and tube anode: Rh. The error of the XRF method was found to be ±1 wt %. The spectra were processed using the method of fundamental parameters. The target and measured elemental composition data are given in Table 1.

The morphology of the surface for support and catalysts was demonstrated using a scanning electron microscope (SEM). The analytic measurements were optimized using a target-oriented approach, with the samples mounted on a 25 mm aluminum specimen stub and secured with a conductive adhesive tape prior to measurements. The morphology of the samples was studied under native conditions to rule out metal coating surface effects. The Hitachi SU8000 field-emission scanning electron microscope was used for the observations (FE-SEM). Images were captured in secondary electron mode at a voltage of 10 kV and a working distance of 8−10 mm.[39,40]

https://doi.org/10.1021/acsomega.2c03082
ACS Omega 2022, 7, 21346−21356

Table 2. Texture Properties of Supports and Sulfide Catalysts Supported on Powder Activated Carbons

sample	S_{total}, m^2/g	S_{micro}, m^2/g	S_{meso},[a] m^2/g	V_{total}, cm^3/g	V_{micro}, cm^3/g	V_{meso},[b] cm^3/g	average pore diameter (nm)
DAC	724	662	62	0.34	0.28	0.059	3.2
OBC-1	711	660	51	0.32	0.27	0.046	3.8
$KCoMoS_2$/DAC	250	243	7	0.11	0.10	0.005	3.3
$KCoMoS_2$/OBC-1	178	142	35	0.09	0.06	0.033	3.2

[a] $S_{meso} = S_{total} - S_{micro}$. [b] $V_{meso} = V_{total} - V_{micro}$

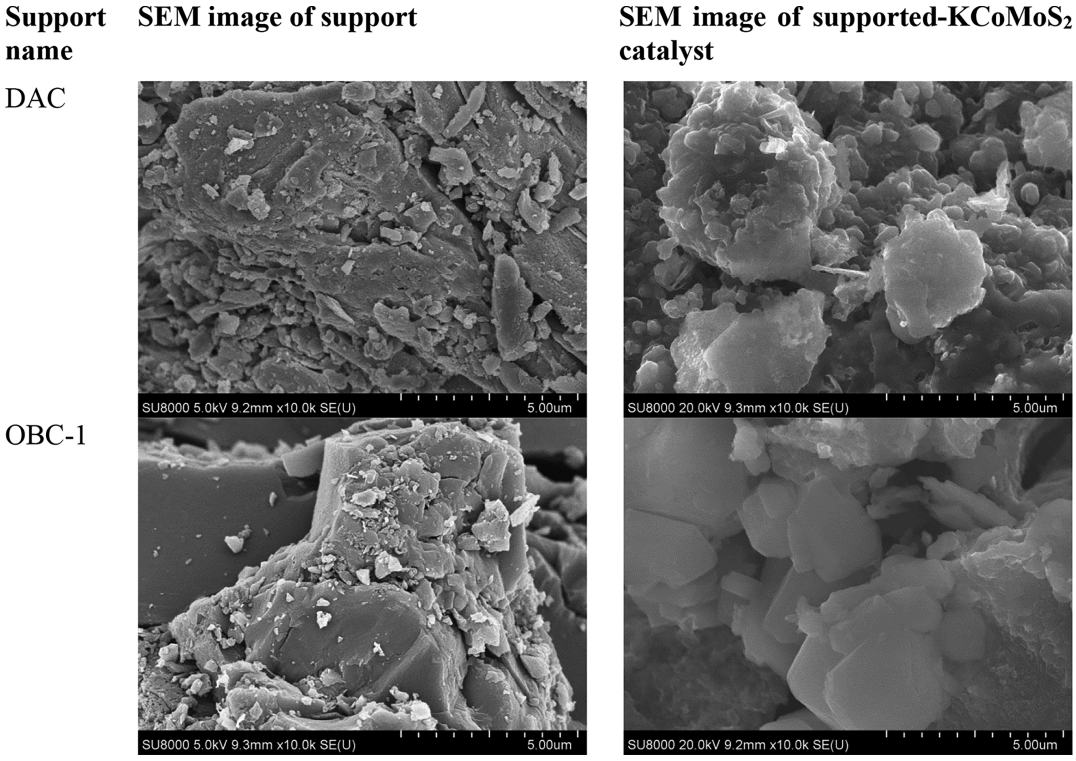

Figure 1. SEM images of powder activated carbon supports and supported $KCoMoS_2$ catalysts.

To determine the morphology of the catalysts, a transmission electron microscope (TEM) was used with two different LaB6 cathodes, one with a 200 kV accelerating voltage and the other with a 300-kV one (FEI Company, USA), to characterize the morphology of the catalysts.

The sulfided catalysts were analyzed by XPS using a Kratos Axis Ultra DLD spectrometer with a monochromatic AlK*source (h* = 1486.6 eV, 150 W). Individual spectral regions were analyzed to determine the binding energy (BE) of the peaks, identify the chemical state of the elements, and calculate relative ratios of the elements on the catalyst surface. The BE values referred to the positions of the Au $4f_{7/2}$ peak at 83.96 eV and the Cu $2p_{3/2}$ peak at 932.62 eV. To survey photoelectron spectra, narrow spectral regions (Al 2p, S 2p, Mo 3d, C 1s, O 1s, and Co 2p) were recorded. The collected spectra were processed by a mixed Gaussian (30%)−Lorentzian (70%) method with the use of the CasaXPS software. Shirley background subtraction was applied to calculate atomic concentrations. The decomposition of the S 2p and Mo 3d XPS spectra was performed using appropriate oxide and sulfide references as supported monometallic catalysts.[41]

2.3. HAS from Syngas over Supported $KCoMoS_2$ Catalysts. The tubular flow reactor via the HAS system was used to synthesize alcohols from syngas. Each catalyst was weighed (3 g) with particle size of 0.2−0.5 mm under the following conditions: volume ratio of syngas: $H_2/CO/Ar$ = 45:45:10%, P = 5.0 MPa, T = 300−360 °C, and weight space velocity = 760 L h^{-1} (kg cat)$^{-1}$. The experiment was performed during 16 h. The reactor temperature was increased to 300 °C over 4 h. The temperature was increased by the ratio 20 °C/4 h. The gaseous products were analyzed every 4 h by two TCD-GC 1 m columns packed with a CaA molecular sieve and Porapak Q, and liquid products were analyzed by FID-GC, 25 m OV-101, and 25 m terephthalic acid/polyethylene glycol columns. The CO(X) conversion was calculated as follows (eq 1):

$$X_C(\%) = 1 - \frac{n_{CO}^{\text{after reaction}}}{n_{CO}^{\text{in feed}}} \times 100 \quad (1)$$

where X_C = syngas conversion and $n_{CO}^{\text{in feed}}$ and $n_{CO}^{\text{after reaction}}$ are the CO content in feed and products (% mol).

The selectivity is calculated on a CO_2-free basis approximation because the CO_2 is formed by a water gas shift reaction (H_2O + CO), constantly affecting the selectivity of final products. CO_2-free selectivity was calculated by eq 2:

$$S_i^{CO_2-\text{free}}(\%) = \frac{S_i}{1 - S_{CO_2}} \times 100 \quad (2)$$

https://doi.org/10.1021/acsomega.2c03082
ACS Omega 2022, 7, 21346−21356

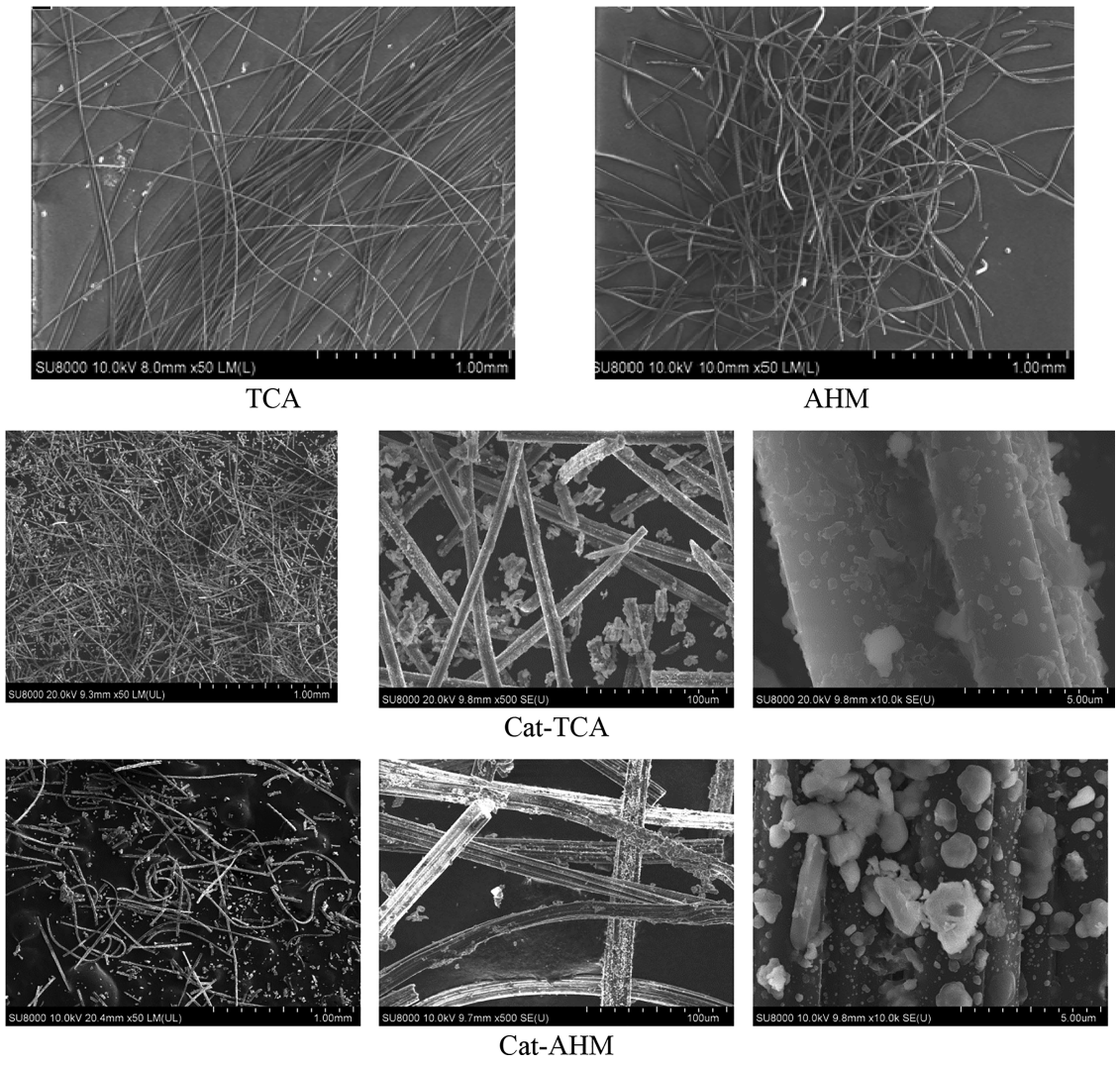

Figure 2. SEM images of the fabric active sorption (TCA), nonwoven activated material (AHM), and their catalysts Cat-TCA and Cat-AHM at high magnification (5 mm) and low magnifications (100 μm and 1 mm).

where $S_i^{CO_2\ -\ free}$ is CO_2 free selectivity to the *i* component, S_i is the selectivity to the *i* component, and S_{CO_2} is the CO_2 selectivity.

3. RESULTS AND DISCUSSION

Table 2 shows the results for the surface area, total pore volume, average pore diameter, micro- and mesopore surface areas, and micro- and mesopore volumes of the stabilized catalysts in sulfide form.

The powder commercial activated carbons DAC and OBC-1 showed a BET surface area of 724 and 711 m^2/g and a total pore volume of 0.34 and 0.32 cm^3/g. Impregnating the AC supports by the KCoMoS active phase decreased the surface area to 250 and 178 m^2/g and total pore volumes to 0.11 and 0.09 cm^3/g. Furthermore, the average pore diameter of DAC increased after being impregnated by the active phase from 3.1 to 3.3 nm, but it decreased from 3.78 to 3.2 nm in the case of OBC-1. A decrease in BET surface area, pore volume, and pore diameter of the catalysts when compared to pure supports indicates that the added metal particles have blocked the pores. Although both powdered activated carbon supports have almost the same porous characteristics, the KCoMoS active phase took different places. In the case of Cat-DAC, the metal species fell on the mesopores, which led to the formation of a microporous catalyst with a smaller mesopore surface area (7 m^2/g) compared with Cat-OBC-1 (35 m^2/g).

The surface morphologies that are characterized by SEM of powder commercial activated carbon supports of DAC, OBC-1, and the catalysts Cat-DAC and Cat-OBC-1 are presented in Figure 1, whereas the SEM images of fabric active sorption (TCA), nonwoven activated material (AHM), and their catalysts Cat-TCA and Cat-AHM are shown in Figure 2.

Figure 1 illustrates the surface morphology of the powder activated carbon (DAC and OBC-1) before and after impregnation by the KCoMoS active phase. As seen in Figure 1, before the impregnation, the surface morphology of powder activated carbons has uneven cavities and fine open pores. An irregular structure and developed pores can be seen after impregnation by the KCoMoS active phase, which has a smoother surface of activated carbon. The development of pores can be due to the effect of the KCoMoS active phase that has filled the pores. Also, more holes and pits are noted.

From the SEM images shown in Figure 2, it can be observed that the fabric active sorption and nonwoven activated material ACs present a filamentous morphology with a strip axial arrangement and that a few longitudinal grooves and many

https://doi.org/10.1021/acsomega.2c03082
ACS Omega 2022, 7, 21346−21356

irregular particles are distributed on the fiber surfaces. Otherwise, the degree of entanglement of the strip axial arrangement in AHM was found to be more than that in TCA. The SEM images of the catalysts reveal that the surface of fiber activated carbon is smoother after impregnation by the KCoMoS active phase. Some axial wedge fractures are also observed, but the longitudinal texture and porosity of fiber ACs are still retained.

The energy dispersive X-ray (EDX) spectrum of supported $KCoMoS_2$ catalysts is depicted in Supporting Information Figure S1, and the distribution maps of powder and fiber activated carbons are depicted in Figures S2 and S3. The EDS analysis reveals that the composite consists primarily of the KCoMoS active phase, carbon, and oxygen. According to the results, Cat-DAC has also been found to include trace elements such as Si, Fe, Ni, Cr, and P, which can be attributed to the commercial activated carbon support. There are strong signals around 2.5 keV attributed to the Mo and S elemental distribution, which are similar to the EDX study results of MoS_2 catalysts in ref 42. Although there are small differences between the targeted percentage of elements and the detected percentage by EDX, this technique is not useful for quantitative analysis because the complete spectrum is obtained very quickly and the spectrum contains both semiqualitative and semiquantitative information.[43,44] That is why we have adopted the elementary composition results that are obtained from XRF as real and more accurate results (Table 1). The EDX maps of sulfide catalysts supported on powder activated carbon at 2.5 μm are presented in Figure S2.

Cat-DAC and Cat-OBC1 catalysts show slight differences in the EDX maps shown in Figure S2. The distribution maps of S, Co, Mo, and K obtained on the surface of the $KCoMoS_2$ catalyst coincide completely, indicating that the elements form a unified phase.

The agglomeration of KCoMoS active phase elements in fiber activated carbons (Figure 2 and Figure S3) was found to be more than that of powder activated carbons (Figure 1 and Figure S2). Representative TEM micrographs of the supported $KCoMoS_2$ catalysts are shown in Figure 3.

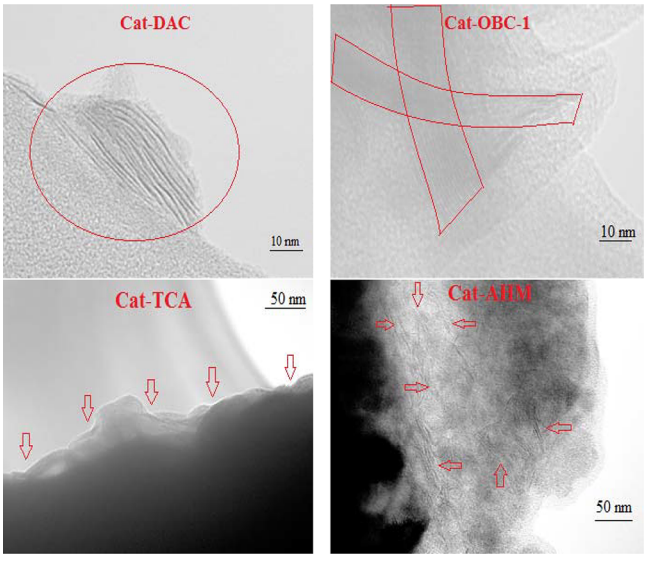

Figure 3. TEM images of the supported $KCoMoS_2$ catalysts.

The MoS_2 slabs appear clearly as threadlike fringes in multilayer particles of the KCoMoS active phase with different stacking degrees. The differences between the catalysts' understudy can be attributed to the interaction between the KCoMoS active phase and activated carbons.[45,46] Moreover, the MoS_2 crystallites formed a filamentous morphology on the surface of fiber activated carbons (TCA and AHM). The surface of AHM is more tangled compared with that of TCA, thus leading to the formation of tangled MoS_2 slabs on AHM and long linear slabs on TCA with long rim sites. It is notable that increasing the stacking degree leads to an increase in vacancies and corner sites in the active phase, which decreases the adsorption of hydride hydrogen,[46,47] whereas increasing the rim sites of MoS_2 slabs promotes the hydrogenation reaction.[48,49]

Chemical species present on the surface of the $KCoMoS_2$ supported catalysts were evaluated by XPS. Figure 4 shows

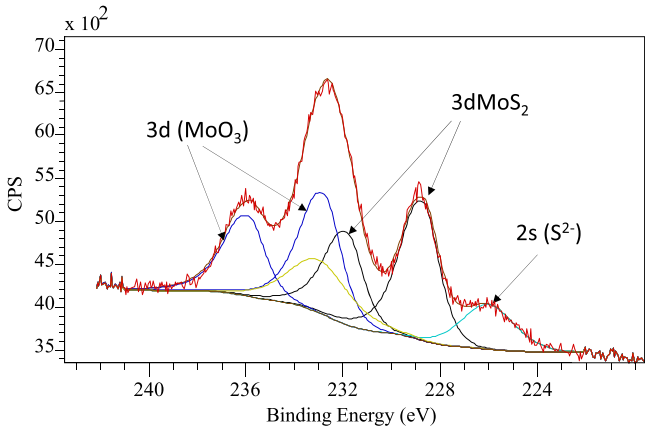

Figure 4. XPS Mo 3d spectra for the sulfided $KCoMoS_2$/OBC-1 catalyst.

typical XPS spectra for the Mo 3d region. The Mo 3d spectra contain two Mo 3d doublets. The Mo $3d_{5/2}$ and $3d_{3/2}$ doublet with BE at 228.7 and 232.0 eV, respectively, corresponds to the Mo^{4+} in the MoS_2 phase species.[41] The doublet with BE equal to 232.8 and 235.9 eV belongs to the Mo^{6+} oxide species. The peak at BE of 226.0 eV is assigned to S 2s.

For all catalysts, the contributions of K $2p_{3/2}$ and S $2p_{3/2}$ at the ranges of 292.5−293.0 and 162.0 eV, respectively, were also detected and corresponded to K^+ and S_2- states.[50,51] In the sulfur spectra, there was also a contribution of SO_4^{2-} observed that is ordinary for K-doped TMS catalysts. The sulfidation degree of the metal (Table 3) was equal for all the samples; relative concentrations of MoS_2 and CoS_x (CoMoS) were in the range of 50−55 and 30−35 rel %.

Table 3. Sulfidation Degree of Mo and Co at the Catalyst Surface from XPS

	sulfidation degree of metal (%)		
sample	Mo	Co	S/(Mo + K + Co) at ratio
$KCoMoS_2$/DAC	54	32	1.3
$KCoMoS_2$/OBC-1	52	30	0.9
$KCoMoS_2$/TCA	56	31	1.0
$KCoMoS_2$/AHM	55	35	1.5

https://doi.org/10.1021/acsomega.2c03082
ACS Omega 2022, 7, 21346−21356

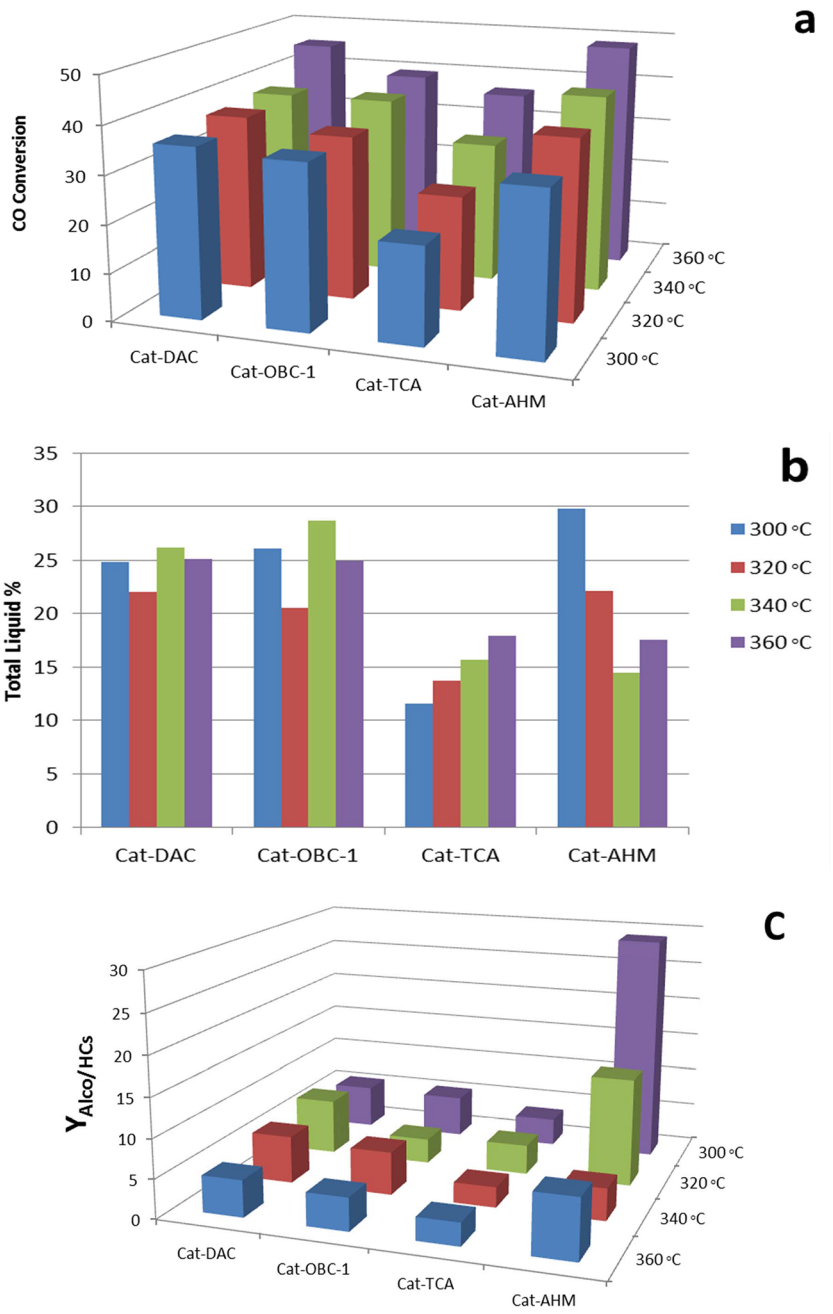

Figure 5. The HAS results of supported $KCoMoS_2$ catalysts. (a) CO conversion, (b) total liquid yield, and (c) yield ratio between alcohols and hydrocarbons. The conditions are T = 300−360 °C, P = 5 MPa, GHSV = 760 L h^{-1} (kg cat)$^{-1}$, and H_2/CO = 1.0.

The catalytic performance of supported $KCoMoS_2$ catalysts at 300, 320, 340, and 360 °C is presented on Figure 5 and Table S1 in the Supporting Information.

The main reasons for syngas conversion results can be attributed to the clear differences in the surface morphologies of the supports and catalysts and the degree of interaction between the support and active phase. Obtained results in Figure 5a reveal that a positive correlation between CO conversion and temperatures of the catalysts under study has been observed. The CO conversation increases in the order Cat-TCA < Cat-OBC-1 < Cat-DAC < Cat-AHM. Claure *et al.*[45] and Niannian *et al.*[47] concluded that MoS_2 catalysts with short MoS_2 layers had a higher selectivity for syngas conversion and HAS. Based on these reports, we believed that these short and thin layers for the Cat-AHM catalyst could increase the ratios of the basal, corner, and surface sides of the catalyst, which produces more active sites and then improves the catalytic activities, particularly HAS. In contrast, the lowest catalytic activities of Cat-TCA can be attributed to the long linear slabs that have formed on the strip axial arrangement surface of TCA commercial activated carbon. In our previous work,[52−54] we found an unusual correlation between catalytic performances of supported-$KCoMoS_2$ and the micro- and mesopore structure of the catalyst support. It was found that catalysts supported on microporous materials possessed a higher catalytic activity in HAS synthesis from syngas than those supported on mesoporous materials. The catalytic performance results in Figure 5a−c of powder activated carbons (Cat-DAC and Cat-OBC-1) corroborate the validity of this unusual finding because the microporous Cat-DAC with

https://doi.org/10.1021/acsomega.2c03082
ACS Omega 2022, 7, 21346−21356

Table 4. Comparison of Support Nature, Reaction Conditions, and Catalytic Properties in HAS from Synthesis Based on $KCoMoS_2$ Catalysts Taken from the Literature with the Current Study

			reaction conditions						
type of support	active phase	preparation method	P (MPa)	T (°C)	GHSV (h^{-1})	H_2/CO	CO (%)	total liquid selectivity (%)	ref
unsupported	KCoMoS	hydrothermal synthesis	6.0	340	2000	2	29	30	46
unsupported		coprecipitation					35	35	
unsupported		reverse microemulsion					39	60	
Al_2O_3		wetness impregnation	5.0	340	760	1	23	48	57
Al_2O_3/C (≈1%)			5.0	340	760	1	19.2	65	27
MWCNT			8.3	320	1200	1	25	40	58
AC-Darco[a]			8.27	330	1200	2	35.6	24.8	36
AC-RX3 extra[b]							39.6	25.8	
AC-CGP super[c]							44.5	27.5	
Current Cat-DAC			5.0	360	760	1	45.3	55.3	
Current Cat-OBC-1							39.3	54	
Current Cat-TCA							36.36	48.7	
Current Cat-AHM							48.5	63.4	

[a]AC-Darco is an activated carbon purchased from Aldrich, Canada. [b]AC-RX3 is a commercial AC obtained from Norit, USA. [c]AC-CGP Super is a commercial AC obtained from Norit, USA.

Table 5. The Yield of Hydrocarbons, Carbon Dioxide, and Each Alcohol

T (°C)	C1 (%)	CO_2 (%)	C2 (%)	C3 (%)	C4 (%)	MeOH (%)	EtOH (%)	PrOH-1 (%)	BuOH-1 (%)	i-BuOH (%)	AmOH-1 (%)	i-AmOH (%)
							Cat-DAC					
300	1.5	4.4	1.6	2.0	1.3	4.0	10.6	5.9	1.8	1.3	0.5	0.6
320	0.7	4.5	1.1	2.4	0.4	4.6	12.0	6.7	2.0	1.5	0.6	0.7
340	1.3	7.2	1.3	0.8	0.9	4.3	11.2	6.2	1.9	1.4	0.5	0.7
360	2.4	11.9	2.0	1.0	0.3	4.1	10.7	6.0	1.8	1.4	0.5	0.7
							Cat-OBC-1					
300	0.1	4.5	1.1	2.2	0.6	5.9	9.1	5.8	1.6	2.3	0.4	0.8
320	0.5	4.9	1.2	3.1	1.6	4.7	7.2	4.6	1.3	1.8	0.3	0.6
340	0.1	5.3	0.2	3.2	0.3	6.6	10.1	6.4	1.8	2.6	0.5	0.8
360	1.9	8.4	1.3	0.9	1.7	5.7	8.8	5.6	1.5	2.2	0.4	0.7
							Cat-TCA					
300	1.0	5.4	1.5	0.4	0.4	2.3	5.2	2.2	0.7	0.6	0.2	0.4
320	1.6	6.6	1.4	0.3	0.3	2.7	6.2	2.6	0.9	0.7	0.2	0.4
340	2.3	8.6	1.9	0.8	0.4	3.1	7.1	3.0	1.0	0.8	0.3	0.5
360	3.7	12.0	0.4	1.8	1.0	3.5	8.0	3.4	1.1	0.9	0.3	0.6
							Cat-AHM					
300	0.0	3.2	0.3	0.0	0.0	4.9	11.9	7.3	2.1	2.1	0.5	1.0
320	0.4	3.0	0.8	0.4	0.0	4.0	9.0	5.0	2.0	2.0	0.0	0.1
340	1.7	5.6	1.0	0.6	1.1	3.0	9.1	1.3	0.4	0.4	0.1	0.2
360	0.8	5.7	0.9	0.3	0.3	2.9	8.1	4.3	1.2	1.2	0.3	0.6

smaller mesopores was found to be more active than Cat-OBC-1 with higher mesopores (see Table 2 and Figure 5). Surisetty *et al.*[36] have reported that the dispersion of KCoMoS on mesoporous MWCNT is lower than that on microporous AC. Enlightened by such a report, we deemed that the lower catalytic performances of Cat-OBC-1 compared with Cat-DAC-1 can be attributed to the agglomeration of the active phase; OBC-1 formed a higher agglomerate compared with DAC (see Figure 1 and Figure S2), thus increasing the rim sides and coupling the important sides of HAS (basal, corner, and surface sides).[55−57] Figure 5b revealed that there is no clear correlation between temperature and total liquid yield. Moreover, the $KCoMoS_2$ catalysts supported powder ACs (Cat-DAC and Cat-OBC-1) yielded more total liquids than fiber ACs (Cat-TCA and Cat-AHM). The highest TLY% was observed for Cat-AHM at 300 °C. From Figure 5c, the highest $Y_{Alco/HCs}$ was achieved at 340 °C for powder ACs, whereas it was at 300 °C for fiber AC supported catalysts. It can be seen that the $Y_{Alco/HCs}$ displayed the descending order of Cat-AHM > Cat-DAC > OBC-1 > Cat-TCA. The current results were compared with several studies of HAS from syngas over supported and unsupported $CoMoS_2$ catalysts (see Table 4). In addition, the catalyst was not deactivated at the end of the reaction, indicating that it is stable and repeatable.

The obtained results indicate that the current novel commercial activated carbons are a promising support for the field of HAS because the $KCoMoS_2$ catalysts supported on novel commercial activated carbons (DAC, OBC-1, TCA, AHM) show the best CO conversion and TLY% at the optimum conditions compared with published studies on the same field (see Table 4), except for the results of unsupported $KCoMoS_2$ prepared by the reverse microemulsion method.[47] However, this method is considered expensive compared with the used wetness impregnation method, which is considered to

https://doi.org/10.1021/acsomega.2c03082
ACS Omega 2022, 7, 21346−21356

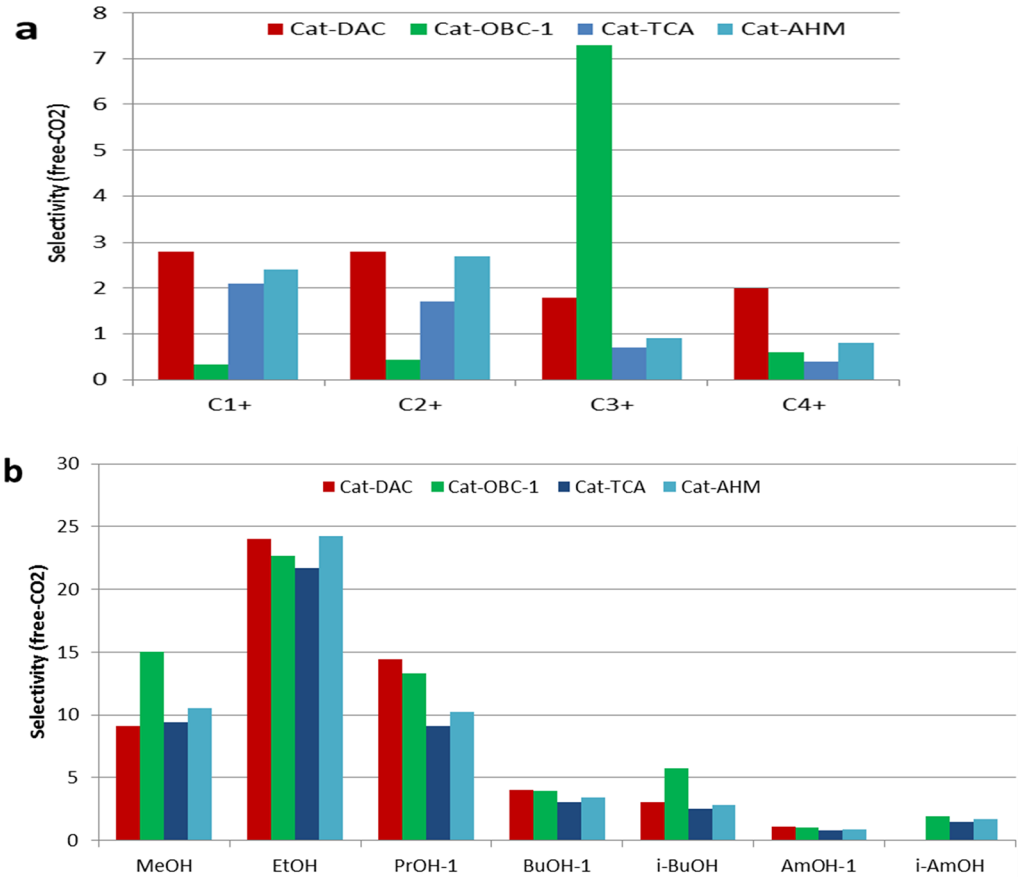

Figure 6. Product selectivity of supported catalysts toward (a) light hydrocarbons (C1−C4) and (b) methanol, ethanol, propanol-1, amyl alcohol, butanol-1, isobutanol, and isoamyl alcohol. Reaction condition: H_2/CO = 1.0, GHSV = 760 L h^{-1} (kg cat)$^{-1}$, T = 340 °C, and P = 5 MPa.

be of high feasibility, and it was used in many methods of preparing catalysts in the field of the petrochemical industry and treatment of petroleum products. The gaseous and alcohol product yields of syngas conversion are presented in Table 5.

The nature of the carriers used in the higher alcohol synthesis has a bearing on the extent of alcohol product distribution. Furthermore, the morphology and structure of the support would directly affect its porosity and the ease of modifying its surface characteristics by functionalization.[59] As a result, the ability of the supports to disperse active metal species on the support can be influenced by their interaction with the KCoMoS active phase. It is quite obvious that the products generated by DAC, OBC-1, TCA, and AHM-supported $KCoMoS_2$ catalysts investigated consisted mostly of light hydrocarbons (C1−C4), linear alcohols with carbon numbers in the range of C1 to C5, a small amount of iso-alcohol, and carbon dioxide that is produced from the reaction between CO and vapor water. As can be seen, the yield of hydrocarbons and CO_2 showed a positive correlation with the temperature, whereas the yield of each alcohol did not appear to have any correlation with the temperature. The highest yield for methane and carbon dioxide recorded over Cat-TCA, whereas Cat-DAC showed the highest yield of ethane, and for propane and butane Cat-OBC-1 showed the best yield. Moreover, the total yield of hydrocarbons at 360 °C followed the trend Cat-TCA (6.9%) > Cat-OBC-1 (5.9%) > Cat-DAC (5.6%) > Cat-AHM (2.3%). Ethanol, propanol-1, and methanol were the most predominant alcohol products in the final liquid products, with the byproducts comprising mainly of butanol-1, isobutanol, amyl alcohol, and isoamyl alcohol. Propanol-2 and butanol-2 were not synthesized over supported $CoMoS_2$ catalysts at all reaction conditions. These results are considered different compared with previous studies that have used activated carbons as support for HAS form syngas over K-modified $CoMoS_2$ catalysts.[24,36,52−54] The order of catalysts for synthesizing each alcohol is as follows: for ethanol, propanol-1, and butanol-1: Cat-DAC > Cat-AHM > Cat-OBC-1 > Cat-TCA; for methanol: Cat-OBC-1 > Cat-DAC > Cat-AHM > Cat-TCA; for amyl alcohol-1: Cat-DAC > Cat-OBC-1 > Cat-AHM > Cat-TCA; and for isobutanol and isoamyl alcohol: OBC-1 > TCA > DAC > AHM. The selectivity toward light hydrocarbons and alcohols is presented in Figure 6.

In the current investigation, the role of the support on product selectivity was studied. The selectivity for C_{1+} and C_{2+} was found to be higher than that for C_{3+} and C_{4+} for all catalysts, except for the highest selectivity of Cat-OBC-1 toward C_{3+}, these results attributed to the mesoporosity of Cat-OBC-1, which occurs more acid sites with the part-cover of MoS_2 crystallite edges, besides the active phase agglomeration, which suggests a somewhat higher hydrogenation ability with more isomerization. The powdered activated carbon supported catalysts (Cat-DAC and Cat-OBC-1) show a higher selectivity than fiber activated carbons (Cat-TCA and Cat-AHM) toward C_{3+}, C_{4+}, propanol-1, butanol-1, isobutanol, and amyl alcohol-1. In contrast, the highest selectivity for ethanol appears over Cat-AHM, which might be attributed to the higher stacking number of the MoS_2 crystallite as a result of the

https://doi.org/10.1021/acsomega.2c03082
ACS Omega 2022, 7, 21346−21356

tangled surface morphology of AHM, which led to the formation of considerable amounts of vacancies and corner sites that support higher alcohol selectivity in general and ethanol in particular. For powdered activated carbons, the catalyst that contains the highest micropores (Cat-DAC) produced a considerable amount of linear alcohols compared with Cat-OBC-1. Microporous catalysts inhibit isomerization due to steric constraints. The latter finding is consistent with our previous results in refs 52−54. This interpretation did not apply to the methanol synthesis over Cat-OBC-1 because it possessed a more mesoporous structure. We presumed that the difference in the porosity of the catalysts did not affect the methanol synthesis due to the small size of CH_3^+ and its stereo structure, so it could be easily adsorbed compared with other linear alcohols.

4. CONCLUSIONS

In summary, the role of powder ACs with different textural characteristics (Cat-DAC and Cat-OBC-1) and fiber ACs (TCA and AHM) as supports for HAS from syngas over K-modified $CoMoS_2$ catalysts was studied. The catalytic performances of powder activated carbons corroborate the validity of the unusual correlation between porosity and catalytic activity because the microporous Cat-DAC with smaller mesopores was found to be more active than Cat-OBC-1 that possesses higher mesopores. For powdered activated carbons, the catalyst that contains the highest micropores (Cat-DAC) produced a considerable amount of linear alcohols compared with Cat-OBC-1.

The short and thin layers of the Cat-AHM catalyst increased the corner, basal, and surface sides of the catalyst, which forms more active MoS_2 crystallites and then increases the catalytic activities, particularly HAS. In contrast, the lowest catalytic activities of Cat-TCA can be attributed to the long linear slabs that form on the strip axial arrangement surface of the TCA commercial activated carbon.

■ ASSOCIATED CONTENT

Supporting Information

The Supporting Information is available free of charge at https://pubs.acs.org/doi/10.1021/acsomega.2c03082.

The energy dispersive X-ray (EDX) map sum spectrum of supported-$KCoMoS_2$; EDX maps of the $KCoMoS_2$ catalysts supported on powder commercial activated carbons; EDX maps of the $KCoMoS_2$ catalysts supported on fiber commercial activated carbons; HAS results of supported-$KCoMoS_2$ catalysts under the same conditions; CO conversion; total liquid yield; and yield ratio between alcohols and hydrocarbons (PDF)

■ AUTHOR INFORMATION

Corresponding Author

Mohamed E. Osman − *Peoples' Friendship University of Russia, Moscow 117198, Russia; N.D. Zelinsky Institute of Organic Chemistry RAS, Moscow 119991, Russia;* orcid.org/0000-0003-4662-062X; Email: wadalmsna3.com@gmail.com

Authors

Vladimir V. Maximov − *N.D. Zelinsky Institute of Organic Chemistry RAS, Moscow 119991, Russia*

Tshepo D. Dipheko − *Peoples' Friendship University of Russia, Moscow 117198, Russia; N.D. Zelinsky Institute of Organic Chemistry RAS, Moscow 119991, Russia*

Tatiana F. Sheshko − *Peoples' Friendship University of Russia, Moscow 117198, Russia*

Alexander G. Cherednichenko − *Peoples' Friendship University of Russia, Moscow 117198, Russia*

Pavel A. Nikulshin − *All-Russia Research Institute of Oil Refining, Moscow 111116, Russia;* orcid.org/0000-0002-3243-7835

Victor M. Kogan − *N.D. Zelinsky Institute of Organic Chemistry RAS, Moscow 119991, Russia*

Complete contact information is available at: https://pubs.acs.org/10.1021/acsomega.2c03082

Notes

The authors declare no competing financial interest.

■ ACKNOWLEDGMENTS

The publication was carried out with the support of the Strategic Academic Leadership Program of the RUDN.

■ REFERENCES

(1) Subramani, V.; Gangwal, S. K. A review of recent literature to search for an ecient catalytic process for the conversion of syngas to ethanol. *Energy Fuels* **2008**, *22*, 814−839.

(2) Forzatti, P.; Tronconi, E.; Pasquon, I. Higher Alcohol Synthesis. *Catal. Rev.* **1991**, *33*, 109−168.

(3) Dalmon, J. A.; Chaumette, P.; Mirodatos, C. Higher alcohols synthesis on cobalt based model catalysts. *Catal. Today* **1992**, *15*, 101−127.

(4) Xi, X.; Zeng, F.; Cao, H.; Cannilla, C.; Bisswanger, T.; de Graaf, S.; Pei, Y.; Frusteri, F.; Stampfer, C.; Palkovits, R.; Heeres, H. J. Enhanced C_{3+} alcohol synthesis from syngas using KCoMoSx catalysts: effect of the Co-Mo ratio on catalyst performance. *Appl. Catal., B* **2020**, *272*, No. 118950.

(5) Camposmartin, J. M.; Guerreroruiz, A.; Fierro, J. L. G. Structural and Surface Properties of CuO-ZnO-Cr_2O_3 Catalysts and Their Relationship with Selectivity to Higher Alcohol Synthesis. *J. Catal.* **1995**, *156*, 208−218.

(6) Boz, I.; Sahibzada, M.; Metcalfe, I. S. Kinetics of the Higher Alcohol Synthesis over a K-promoted CuO/ZnO/Al_2O_3 Catalyst. *Ind. Eng. Chem. Res.* **1994**, *33*, 2021−2028.

(7) Zhang, H.; Yang, X.; Zhou, L.; Su, Y.; Liu, Z. Conversion of syngas to higher alcohols over Cu-Fe-Zr catalysts induced by ethanol. *J. Nat. Gas Chem.* **2009**, *18*, 337−340.

(8) Srivastava, S.; Jadeja, G. C.; Parikh, J. A versatile bi-metallic copper−cobalt catalyst for liquid phase hydrogenation of furfural to 2-methylfuran. *RSC Adv.* **2016**, *6*, 1649−1658.

(9) Woo, H. C.; Nam, I. S.; Lee, J. S.; Chung, J. S.; Kim, Y. G. Structure and distribution of alkali promoter in K/MoS_2 catalysts and their effects on alcohol synthesis from syngas. *J. Catal.* **1993**, *690*, 142−672.

(10) Toyoda, T.; Minami, T.; Qian, E. W. Mixed alcohol synthesis over sulfided molybdenum-based catalysts energy. *Fuels* **2013**, *27*, 3769−3777.

(11) Li, D.; Yang, C.; Qi, H.; Li, W.; Sun, Y.; Zhong, B. Higher alcohol synthesis over a La promotedNi/K_2CO_3/MoS_2 catalyst. *Catal. Commun.* **2004**, *5*, 605−609.

(12) Saito, M.; Anderson, R. B. The activity of several molybdenum compounds for the methanation of CO. *J. Catal.* **1980**, *63*, 438−446.

(13) Quarderer, G. J.; Cochran, G. Dow Chemical Company, European Patent 0119609, 1984.

(14) Kinkade, N. E. Union Carbide, International Patent WO8503073, 1984.

(15) Permyakov, E. A.; Dorokhov, V. S.; Maximov, V. V.; Nikulshin, P. A.; Pimerzin, A. A.; Kogan, V. M. Computational and experimental study of the second metal effect on the structure and properties of bimetallic MeMoS-sites in transition metal sulfide catalysts. *Catal. Today* **2018**, *305*, 19−27.
(16) Dorokhov, V. S.; Ishutenko, D. I.; Nikul'shin, P. A.; Kotsareva, K. V.; Trusova, E. A.; Bondarenko, T. N.; Eliseev, O. L.; Lapidus, A. L.; Rozhdestvenskaya, N. N.; Kogan, V. M. Conversion of Synthesis Gas into Alcohols on Supported Cobalt− Molybdenum Sulfide Catalysts Promoted with Potassium. *Kinet. Catal.* **2013**, *54*, 253−262.
(17) Surisetty, V. R.; Dalai, A. K.; Kozinski, J. Intrinsic Reaction Kinetics of Higher Alcohol Synthesis from Synthesis Gas over Sulfided Alkali-promoted Co-Rh-Mo Trimetallic Catalyst Supported on MWCNTs. *Energy Fuels* **2010**, *24*, 4130−4137.
(18) Li, Z.; Fu, Y.; Bao, J.; Jiang, M.; Hu, T.; Liu, T.; Xie, Y. Influences of metals on the stacking numbers. *Appl. Catal., A* **2001**, *220*, 21−30.
(19) Kogan, V. M.; Nikulshin, P. A. On the dynamic model of promoted molybdenum sulfide catalysts. *Catal. Today* **2010**, *149*, 224−231.
(20) Escobar, J.; Barrera, M. C.; Gutíerrez, A. W.; Cortés-Jacome, M. A.; Angeles-Chávez, C.; Toledo, J. A.; Solís-Casados, D. A. Highly active P-doped sulfided NiMo/alumina HDS catalysts from Mo-blueby using saccharose as reducing agents precursor. *Appl. Catal., B* **2018**, *237*, 708−720.
(21) Zaman, S.; Smith, K. J. A Review of Molybdenum Catalysts for Synthesis Gas Conversion to Alcohols: Catalysts, Mechanisms and Kinetics. *Catal. Rev.* **2012**, *54*, 41−132.
(22) Tluk, H. T.; Mondelli, C.; Ferré, D. C.; Stewart, J. A.; Pérez-Ramírez, J. Status and prospects in higher alcohols synthesis from syngas. *Chem. Soc. Rev.* **2017**, *46*, 1358−1426.
(23) Li, D.; Yang, C.; Zhao, N.; Qi, H.; Li, W.; Sun, Y.; Zhong, B. *Fuel Process. Technol.* **2007**, *88*, 125−127.
(24) Surisetty, V. R.; Eswaramoorthi, I.; Dalai, A. K. Comparative study of higher alcohols synthesis over alumina and activated carbon-supported alkali-modified MoS_2 catalysts promoted with group VIII metals. *Fuel* **2012**, *96*, 77−84.
(25) Lva, M.; Xie, W.; Sun, S.; Wu, G.; Zheng, L.; Chu, S.; Gao, C.; Bao, J. Activated-carbon-supported K-Co−Mo catalyst for synthesis of higher alcohols from syngas. *Catal. Sci. Technol.* **2015**, *5*, 2925−2934.
(26) Iranmahboob, J.; Hill, D. O.; Toghiani, H. K_2CO_3/Co- MoS_2/clay catalyst for synthesis of alcohol: influence of potassium and cobalt. *Appl. Catal., A* **2002**, *231*, 99−108.
(27) Dorokhov, V. S.; Kamorin, M. A.; Rozhdestvenskaya, N. N.; Kogan, V. M. Synthesis and conversion of alcohols over modified transition metal sulphides. *C. R. Chim.* **2016**, *19*, 1184−1193.
(28) Badwal, S. P. S.; Giddey, S.; Kulkarni, A.; Goel, J.; Basu, S. Direct ethanol fuel cells for transport and stationary applications − A comprehensive review. *Appl. Energy.* **2015**, *145*, 80−103.
(29) Kohl, A.; Linsmeier, C.; Taglauer, E.; Knozinger, H. Influence of Support and Promotor on the. Catalytic Activity of Rh/VOx/SiO_2 Model Catalysts. *Phys. Chem.* **2001**, *3*, 4639−4643.
(30) Tauster, S. J.; Fung, S. C.; Baker, R. T. K.; Horsley, J. A. Strong Interactions in Supported-Metal Catalysts. *Science* **1981**, *211*, 1121−1125.
(31) Hindermann, J. P.; Deluzarche, A.; Kieffer, R.; Kiennemann, A. Characterization of Chemisorbed Species in CO/H_2 and CO_2/H_2 Reactions: Evolutive Behaviour of the Species. *Can. J. Chem. Eng.* **1983**, *61*, 21−28.
(32) Li, D.; Li, R.; Lu, M.; Lin, X.; Zhan, Y.; Jiang, L. Carbon dioxide reforming of methane over Ru catalysts supported on Mg-Al oxides: A highly dispersed and stable Ru/Mg(Al)O catalyst. *Appl. Catal., B* **2017**, *200*, 566−577.
(33) Ma, Z.; Dai, S. Development of novel supported gold catalysts: A materials perspective. *Nano Res.* **2011**, *4*, 3−32.
(34) Hosseinia, S. A.; Taeba, A.; Feyzi, F.; Yaripour, F. Fischer−Tropsch synthesis over Ru promoted Co/γ-Al_2O_3 catalysts in a CSTR. *Catal. Commun.* **2004**, *5*, 137−143.
(35) Zhang, C.; Chen, L.; Cheng, H.; Zhu, X.; Qi, Z. Atomically dispersed Pd catalysts for the selective hydrogenation of succinic acid to γ-butyrolactone. *Catal. Today* **2016**, *276*, 55−61.
(36) Surisetty, R.; Dalai, A. K.; Kozinski, J. Influence of porous characteristics of the carbon support on alkali-modified trimetallic Co−Rh−Mo sulfided catalysts for higher alcohols synthesis from synthesis gas. *Appl. Catal., A* **2011**, *393*, 50−58.
(37) Mukhin, V. M.; Korolev, N. V. Production of Activated Carbon Based on the Coal/Pitch System. *Chem. Sustainable Dev.* **2018**, *26*, 577−581.
(38) Sing, K. S. W.; Moscou, L.; Pierotti, R. A.; Rouquerol, J.; Siemieniewska, T. Reporting Physisorption Data for Gas/Solid Systems with Special Reference to the Determination of Surface Area and Porosity. *Pure App. Chem.* **1985**, *57*, 603−619.
(39) Kachala, V. V.; Khemchyan, L. L.; Kashin, A. S.; Orlov, N. V.; Grachev, A. A.; Zalesskiy, S. S.; Ananikov, V. P. Target-oriented analysis of gaseous, liquid and solid chemical systems by mass spectrometry, nuclear magnetic resonance spectroscopy and electron microscopy. *Russ. Chem. Rev.* **2013**, *82*, 648−685.
(40) Kashin, A. S.; Ananikov, V. P. A SEM study of nanosized metal films and metal nanoparticles obtained by magnetron sputtering. *Russ. Chem. Bull. Int. Ed.* **2011**, *60*, 2602−2607.
(41) Ishutenko, D.; Anashkin, Y.; Nikulshin, P. The effect of carrier in KCoMoS-supported catalysts for hydro-upgrading of model FCC gasoline. *Appl. Catal., B* **2019**, *259*, No. 118041.
(42) Zhu, X.; Liang, X.; Fan, X.; Su, X. Fabrication of flower-like MoS_2/TiO_2 hybrid as an anode material for lithium ion batteries. *RSC Adv.* **2017**, *7*, 38119−38124.
(43) Taheraslani, M.; Gardeniers, H. High-Resolution SEM and EDX Characterization of Deposits Formed by CH_4+Ar DBD Plasma Processing in a Packed Bed Reactor. *Nanomaterials* **2019**, *9*, 589.
(44) Reed, S. J. B. *Electron Microprobe Analysis*, 2nd ed; Cambridge University Press: Cambridge; 1993; pp. 166−180.
(45) Claure, M. T.; Chai, S. H.; Dai, S.; Unocic, K. A.; Alamgir, F. M.; Agrawal, P. K.; Jones, C. W. Tuning of higher alcohol selectivity and productivity in CO hydrogenation reactions over K/MoS_2 domains supported on mesoporous activated carbon and mixed MgAl oxide. *J. Catal.* **2015**, *97*, 324−388.
(46) Lee, J. J.; Han, S.; Kim, H.; Koh, J. H.; Hyeon, T.; Moon, S. H. Performance of CoMoS catalysts supported on nanoporous carbon in the hydrodesulfurization of dibenzothiophene and 4,6-dimethyldibenzothiophene. *Catal. Today* **2003**, *86*, 141−149.
(47) Niannian, Q.; Xiaoliang, M.; Lu, Z.; Kegong, F. Effect of $KCoMoS_2$ Catalyst Structures on the Catalytic Performance of Higher Alcohols Synthesis via CO Hydrogenation. *Catalysts* **2020**, *10*, 151−163.
(48) Luan, X.; Yong, J.; Dai, X.; Zhang, X.; Qiao, H.; Yang, Y.; Huang, X. Tungsten-doped molybdenum sulfide with dominant double-layer structure on mixed MgAl oxide for higher alcohol synthesis in CO hydrogenation. *Ind. Eng. Chem. Res.* **2018**, *57*, 10170−10179.
(49) Nikulshin, P. A.; Salnikov, V. A.; Mozhaev, A. V.; Minaev, P. P.; Kogan, V. M.; Pimerzin, A. A. Relationship between active phase morphology and catalytic properties of the carbon−alumina-supported Co(Ni)Mo catalysts in HDS and HYD reactions. *J. Catal.* **2014**, *309*, 386−396.
(50) Cordova, A.; Blanchard, P.; Lancelot, C.; Frémy, G.; Lamonier, C. Probing the Nature of the Active Phase of Molybdenum-Supported Catalysts for the Direct Synthesis of Methylmercaptan from Syngas and H2S. *ACS Catal.* **2015**, *5*, 2966−2981.
(51) Kogan, V. M.; Nikulshin, P. A.; Rozhdestvenskaya, N. N. Evolution and interlayer dynamics of active sites of promoted transition metal sulfide catalysts under hydrodesulfurization conditions. *Fuel* **2012**, *100*, 2−16.
(52) Osman, M. E.; Maximov, V. V.; Dorokhov, V. S.; Mukhin, V. M.; Sheshko, T. F.; Kooyman, P. J.; Kogan, V. M. Carbon-Supported $KCoMoS_2$ for Alcohol Synthesis from Synthesis Gas. *Catalysts* **2021**, *11*, 1321.

https://doi.org/10.1021/acsomega.2c03082
ACS Omega 2022, 7, 21346−21356

(53) Osman, M. E.; Maximov, V. V.; Sheshko, T. F.; Kooyman, P. J.; Mukhin, V. M.; Trusova, E. A.; Kogan, V. M. The role of carbon-containing materials as supports for KCoMoS2 catalyst on synthesis of alcohols from syngas. 1st International Electronic Conference on Catalysis Sciences. *Chem. Proc.* **2020**, *1*, 1−2.
(54) Osman, M. E.; Maximov, V. V.; Dorokhov, V. S.; Popov, M. V.; Sheshko, T. F.; Trusova, E. A.; Kogan, V.M. *Synthesis of higher alcohols from syngas over K-modified CoMoS2 catalyst supported on carbon-containing material*. Catalysis for a Sustainable World Conference, RUDN University, 2020, 22−24.
(55) Daage, M.; Chianelli, R. R. Structure-function relations in molybdenum sulfide catalysts: The "rim-edge" model. *J. Catal.* **1994**, *149*, 414−427.
(56) Morrill, M. R.; Thao, N. T.; Shou, H.; Davis, R. J.; Barton, D. G.; Ferrari, D.; Agrawal, P. K.; Jones, C. W. Origins of unusual alcohol selectivities over mixed MgAl oxide-supported K/MoS_2 catalysts for higher alcohol synthesis from syngas. *ACS Catal.* **2013**, *3*, 1665−1675.
(57) Maximov, V. V.; Permyakov, E.; Dorokhov, V. A.; Wang, Y.; Kooyman, P. J.; Kogan, V. M. Effect of Promoter Nature on Synthesis Gas Conversion to Alcohols over (K)MeMoS_2 /Al_2O_3 Catalysts. *ChemCatChem* **2020**, *12*, 1443−1452.
(58) Surisetty, V. R.; Tavasoli, A.; Dalai, A. K. Synthesis of higher alcohols from syngas over alkali promoted MoS_2 catalysts supported on multi-walled carbon nanotubes. *Appl. Catal., A* **2009**, *365*, 243−251.
(59) Boahene, P. E.; Sammynaiken, R.; Dalai, A. K. Syngas conversion to higher alcohols: application of novel K-promoted coRhMo catalysts supported over carbon nanohorns and its by-products. *Int. J. Petrochem. Sci. Eng.* **2017**, *2*, 1−10.

https://doi.org/10.1021/acsomega.2c03082
ACS Omega 2022, 7, 21346−21356